

# Adaptive Importance Sampling Unscented Kalman Filter With Kernel Regression for SAR Image Super-Resolution

Sithara Kanakaraj<sup>ID</sup>, *Student Member, IEEE*, Madhu S. Nair<sup>ID</sup>, *Senior Member, IEEE*, and Saidalavi Kalady, *Member, IEEE*

**Abstract**—Resolution enhancement of Earth’s images from synthetic aperture radars (SARs), used for applications that require scene interpretations and detailed analysis, fails due to the presence of inherent speckle noise. An inexpensive alternative solution to the problem is to use super-resolution (SR) algorithms that deal with speckle. A novel approach to augment kernel regression into the Adaptive Importance Sampling Unscented Kalman Filter (AISUKF) framework for SAR image SR has been presented in this letter. We have experimented with three different nonlinear kernel regressions, namely, arc-cosine kernel, radial basis function kernel, and steering kernel (SK) regressions. Empirical results suggest that AISUKF with SK regression is more appropriate for the abovementioned SR problem resulting in a better denoised and more detail-preserved output.

**Index Terms**—Kernel regression, steering kernel (SK), super-resolution (SR), synthetic aperture radar (SAR) image, unscented Kalman filter (UKF).

## I. INTRODUCTION

THE radar imaging devices, such as synthetic aperture radar (SAR), generates 2-D and 3-D images of the Earth’s surface for applications, such as land-use monitoring and military surveillance. These images inherently suffer from speckle, which, when super-resolved, would result in poor-quality outputs, causing difficulty in scene interpretation and its analysis. As the updation of technology is expensive, researchers opt for cost-effective alternatives, such as super-resolution (SR) algorithms, to enhance the resolution of these SAR images. SR or resolution enhancement of images can be defined as the transformation of low-resolution (LR) frames into high-resolution (HR) frames, performed either on a single image or multiple images (renders more information) of the same scene. The literature has addressed the SR problem using interpolation techniques [1], learning the LR-HR patches with sparse representation [2]–[4], frequency-domain techniques [5], and using methods from the estimation theory

Manuscript received September 21, 2020; accepted October 12, 2020. Date of publication October 28, 2020; date of current version December 21, 2021. (Corresponding author: Sithara Kanakaraj.)

Sithara Kanakaraj and Saidalavi Kalady are with the Department of Computer Science and Engineering, National Institute of Technology Calicut, Kozhikode 673601, India (e-mail: sitharavp@gmail.com; said@nitc.ac.in).

Madhu S. Nair is with the Artificial Intelligence & Computer Vision Lab, Department of Computer Science, Cochin University of Science and Technology, Kochi 682022, India (e-mail: madhu\_s\_nair2001@yahoo.com).

Digital Object Identifier 10.1109/LGRS.2020.3031600

[6], [7]. A notable work using the estimation theory framework by Wei *et al.* [6] has resolved the elementary computational and storage load problems that exist while using the Kalman Filter (KF) for the SR problem. The presence of speckle that is innate in SAR images limits the application of these general SR techniques on SAR images. Thus, algorithms that handle speckle, in particular, need to be developed for SAR image SR.

We have recently developed an estimation theory-based framework for SAR image SR using the Importance Sampling Unscented Kalman Filter (ISUKF) [8]. This framework was later upgraded as Adaptive Importance Sampling Unscented Kalman Filter (AISUKF) [9] by accounting for the noise covariance statistics. In this letter, we propose a novel approach to correct the Kalman Gain parameter in the AISUKF framework using kernel regression methods. Here, a compensation value is added to the final estimate from the AISUKF framework by learning the relationship between the parameters of the AISUKF model and the residual difference between the prediction from the AISUKF method and the actual value. Three different nonlinear kernel functions—arc-cosine (AC) kernel, radial basis function (RBF) kernel, and steering kernel (SK)—are evaluated and compared for this purpose. The empirical results mentioned in this letter demonstrate an improvement of our current AISUKF framework for SAR image SR [9].

The remaining sections of this letter are organized as follows. Section II briefs the background and the general framework of the resolution enhancement process. The proposed methodology has been elaborated in Section III, and the experimental results along with the observations are discussed in Section IV. Section V concludes this work.

## II. BACKGROUND

The unscented Kalman filter (UKF), a variant of Kalman Filter for nonlinear systems, is based on the unscented transform (UT) principle. The basic objective of UT is to generate sigma points to capture the prior distribution, transform these points through the nonlinearity, and then use them to determine the moments of the posterior distribution. For a random variable  $x$  with dimension  $n_x$ , mean  $\bar{x}$ , and covariance  $P_x$ , the sigma points  $\{S\}$  and its weights  $w^{(\mu)}$  and  $w^{(c)}$  can be

computed as follows:

$$s_i = \begin{cases} \bar{x}, & i = 0 \\ \bar{x} + (\sqrt{(n_x + \lambda)P_x})_i, & i = 1, 2, \dots, n_x \\ \bar{x} - (\sqrt{(n_x + \lambda)P_x})_i, & i = n_x + 1, \dots, 2n_x \end{cases} \quad (1)$$

$$w_0^{(\mu)} = \frac{\lambda}{(n_x + \lambda)}; \quad w_0^{(c)} = w_0^{(\mu)} + (1 - \alpha^2 + \beta) \quad (2)$$

$$w_i^{(\mu)} = w_i^{(c)} = \frac{1}{2(n_x + \lambda)}, \quad 1 \leq i \leq 2n_x \quad (3)$$

where  $\alpha$  decides the spread of sigma points,  $\beta$  incorporates prior knowledge ( $\beta = 2$  for Gaussian distribution), and  $\lambda = \alpha^2(n_x + \kappa) - n_x$ ,  $\kappa \geq 1$ .

The basic UKF model is appended with a Discontinuity-Adaptive Markov Random Field (DA-MRF) prior with importance sampling [10] to account for the speckle present in the SAR images. Using this iterative UKF model, we have developed an SR framework for estimating the pixels in the HR image from the multiple LR images [8]. The input LR images  $y'$  are considered to be the degraded form of the HR image  $\mathcal{H}$  that has been decimated by a factor  $d$  and degraded with a global shift  $F$  and speckle noise with variance  $v$ . The LR images can be mathematically represented as

$$y'_t = dF_t \mathcal{H} * v_t, \quad t = 1, \dots, T \quad (4)$$

where  $T$  is the available number of LR images that aid in the reconstruction of the HR image. Each pixel  $(m, n)$  in the LR image contributes to the reconstruction of the following pixels  $(M, N)$  in the HR frame, where  $M \in \{d \times m - i\}$  and  $N \in \{d \times n - j; 0 \leq i, j \leq d - 1\}$ .

The AISUKF algorithm proposed in [9] incorporates the noise covariance errors into the system. However, it does fail to tackle the errors arising from uncertainty in parameters during the SR procedure in the AISUKF algorithm. In this letter, we propose to include a compensation value to correct the final AISUKF estimate using a kernel regression mechanism. Due to the nonlinear nature of the system, the addition of a constant error correction value is not feasible. Thus, a compensation value for each change in the parameter set has to be generated. The kernel regression mechanism proposed here learns the relation between the AISUKF parameters and the compensation value needed for each pixel in the HR output.

With regard to the nonlinearity of the system, three different nonlinear kernels are experimented and studied to choose the most suitable kernel regression model. We have used two commonly used nonlinear kernels: the Arc-Cosine kernel and the RBF kernel. In addition, we have also used the SK regression model proposed by Takeda *et al.* [11]. This data-adaptive kernel regression method accounts for the spatial sampling density of the data and the actual pixel values of these samples, i.e., it exploits the correlation between the position of the pixels and their values. The size and shape of the kernels adapt locally to the image features, such as edges [11], thereby guaranteeing the preservation of edges in the filtering process. The kernel adaptation is performed by estimating the local gradient between the neighboring values of a pixel and then using this measure to assign weights to the

pixels correspondingly. A higher value is assigned to pixels in the near neighbors of the pixel undergoing the filtering process, thereby assuring recovery of high-frequency information. The proposed technique is described in Section III.

### III. PROPOSED METHOD

We begin the iterative UKF based SR process by registering the LR images using a subpixel registration algorithm [12], to account for the global shift between the LR frames, and by determining the unknown noise variance that exists in the LR frame using a patch-based noise level estimator [13]. The first two moments (mean  $\hat{\mu}$  and variance  $\hat{\sigma}^2$ ), predicted from the DA-MRF prior, along with the noise variance ( $\sigma_v^2$ ) obtained are taken as the initial estimates ( $\bar{z}_0, P_0$ ) for the iterative procedure

$$\bar{z}_0 = [\hat{\mu} \quad 1]^T \quad P_0 = \begin{bmatrix} \hat{\sigma}^2 & 0 \\ 0 & \sigma_v^2 \end{bmatrix}. \quad (5)$$

To predict the pixel intensity at position  $(M, N)$  in the HR output, an initial estimate is computed using (5). These estimates progress through an iterative procedure consisting of the prediction step and updation step. In the prediction step, a set of sigma points and their weights are computed using the estimates from the previous iteration as in (1)–(3). We have set  $\alpha = 1$ ,  $\beta = 0$ , and  $\kappa = 0$ . Consecutively, these sigma points are used to estimate the prior intensity  $\bar{z}_{t|t-1}^1$  and the error covariance  $P_{t|t-1}^1$  as indicated in Algorithm 1. This is followed by the updation step, wherein a new set of sigma points are calculated using the estimate from the prediction step,  $\bar{z}_{t|t-1}^1$ . These new points are then used to compute the intensity estimate  $\bar{z}_{t|t-1}^2$ , innovation covariance ( $P_{IC}$ ), and cross-covariance ( $P_{CC}$ ), as indicated in [9, eqs. (10)–(11)] to aid in the computation of the Kalman gain

$$KG = P_{CC} * (P_{IC})^{-1} \quad (6)$$

$$\bar{z}_t = \bar{z}_{t|t-1}^1 + KG(x_t - \bar{z}_{t|t-1}^2) \quad (7)$$

$$P_t = P_{t|t-1} - KG * P_{IC} * KG^T \quad (8)$$

where  $x_t$  is the intensity at position  $(m, n)$  of LR image  $y_t$ . This is followed by the calculation of the intensity estimate  $\bar{z}_t$  [see (7)] and error covariance  $P_t$  [see (8)] together with the estimation of noise covariances  $V_t$  and  $Q_t$ , as indicated in [9, eqs. (15)–(18)]. Finally, the iterative procedure halts after  $T$  rounds to produce the pixel intensity estimate at position  $(M, N)$  of the HR frame. After estimating all the pixel intensities, we obtain the initial super-resolved HR image  $H$ . A detailed explanation of the abovementioned procedure has been presented in our previous work [9].

Subsequently, the SK regression [11], a two-stage approach, is applied on the image  $H$ . In the initial stage, a second-order classic kernel regression calculates the image gradients along the vertical ( $\hat{H}_{z1}$ ) and horizontal ( $\hat{H}_{z2}$ ) directions to determine the dominant orientations of the local gradients in the image. In the next stage, the orientation data are used to adaptively steer the local kernels, resulting in elongated, elliptical contours spread along the directions of the local edge structures, thereby providing strong preservation of edge details in the final output. The steering matrices,  $SM_i^{steer}$ , are

defined as follows:

$$\text{SM}_i^{\text{steer}} = h\mu_i C_i^{-\frac{1}{2}} \quad (9)$$

where  $h$  is the global smoothing parameter,  $\mu_i$  is the local density of data samples, and  $C_i$ 's are covariance matrices based on differences in the local gray-level values. The choice of  $C_i$  determines the spread of the kernel function along the local edges [11]. The SK regression with a Gaussian function can be mathematically expressed as

$$K_{\text{SM}_i^{\text{steer}}}(\bar{z}_i - \bar{z}) = \frac{\sqrt{\det(C_i)}}{2\pi h^2 \mu_i^2} \exp\left\{-\frac{(\bar{z}_i - \bar{z})^T C_i (\bar{z}_i - \bar{z})}{2h^2 \mu_i^2}\right\} \quad (10)$$

where  $\bar{z}_i$  is the set of neighbors of the pixel of interest,  $\bar{z}$ , in  $H$ . The regression process is repeated iteratively until a minimum mean-square estimate is obtained [11]. To further denoise the homogeneous regions and preserve edges and other fine details, a discontinuity adaptive nonlocal mean (DANLM) [14] filtering is applied on the image  $\hat{H}$  resulting from SK regression. The pseudocode of the proposed technique is presented in Algorithm 1.

---

**Algorithm 1** AISUKF With SK Regression

---

```

1: Input: LR images  $y'_t$ ;  $t = 1, \dots, T$ 
2: LR images are registered to generate  $y_t$  from  $y'_t$ .
3: for all  $(M, N) \in H$  do
4:   Estimate first two moments  $\bar{z}_0$  and  $P_0$  (Eq.5)
5:   for  $t = 1$  to  $T$  do
6:     Prediction Step
7:     Predict sigma points  $S_{t|t-1}$  for  $\bar{z}_{t-1}$  (Eq.1 – Eq.3)
8:     Compute  $\bar{z}_{t|t-1}^1 = \sum_{i=0}^{2n_z} w_i^{(\mu)} S_{i,t|t-1}$  and
       $P_{t|t-1}^1 = \sum_{i=0}^{2n_z} w_i^{(c)} (S_{i,t|t-1} - \bar{z}_{t|t-1}^1) (S_{i,t|t-1} - \bar{z}_{t|t-1}^1)^T +$ 
       $Q_{t-1}$ 
9:     Updation Step
10:    Predict sigma points  $S_t$  for  $\bar{z}_{t|t-1}^1$  (Eq.1 – Eq.3).
11:    Compute  $\bar{z}_{t|t-1}^2 = \sum_{i=0}^{2n_z} w_i^{(\mu)} S_{i,t}$ 
12:    Calculate the Kalman gain  $KG$  (Eq.6)
13:    Compute estimate  $\bar{z}_t$  and covariance  $P_t$  (Eq.7, Eq.8)
14:    Compute noise covariances  $V_t$ ,  $Q_t$  (Eq.15-18 in [9]).
15:   end for
16:    $H_{(M,N)} = \bar{z}_T$ 
17: end for
18: Calculate gradients  $\hat{H}_{z1}$  and  $\hat{H}_{z2}$  from  $H$  using classic
   kernel regression.
19: for  $i = 1$  to  $iter$  do
20:   Compute Steering Matrix  $C$  using the gradients of  $\hat{H}_{i-1}$ 
21:   Do steering kernel regression to get  $\hat{H}_i$  and its gradients
22: end for
23: Perform DANLM filtering on  $\hat{H}_{iter}$ .
24: Output: High-resolution image.

```

---

We have also experimented with two other nonlinear kernels: the AC kernel and the RBF kernel. The regression results using these kernels are augmented into the system by

modifying (7) as follows:

$$\begin{aligned} \bar{z}_t &= \bar{z}_{t|t-1}^1 + KG(x_t - \bar{z}_{t|t-1}^2) + \Delta z_t, \\ \text{where, } \Delta z_t &= \hat{Z}_t - \bar{z}_t. \end{aligned} \quad (11)$$

$\hat{Z}_t$  is the true value,  $\bar{z}_t$  is the estimate from the AISUKF procedure, and  $\Delta z_t$  is the additive correction to  $\bar{z}_t$ , computed by the regression model. The regression model is initially learned by gathering data samples from images with ground truth. The parameter values from (7) ( $D^x$ ) and its corresponding  $\Delta z_t$  value ( $D^y$ ) from the  $T$  iterations at each position of the data sample in HR are used for learning the model. For a query  $Q^x$ , that consists of  $T$  samples

$$\Delta z_t = \frac{\sum_{i=1}^T K(Q^x, D_i^x) \cdot D_i^y}{\sum_{i=1}^T K(Q^x, D_i^x)} \quad (12)$$

where  $K$  is substituted by the different nonlinear kernels in (13) and (14). The AC kernel [15] is defined as

$$K_{ACK,n}(X, Y) = \frac{1}{\pi} \|X\|^n \|Y\|^n AD_n(\theta) \quad (13)$$

where  $AD$  and  $\theta$  are the angular dependence and angle between the input vectors  $X$  and  $Y$ , respectively, and  $n$  is the order of the kernel function.

The RBF kernel is defined as

$$K_{RBF}(X, Y) = e^{(-\gamma \|X - Y\|^2)}, \quad \gamma > 0 \quad (14)$$

where the value of  $\gamma$  determines the model fitting; an increase in  $\gamma$  results in overfitting of the model, and vice versa.

The regression models plugged into the existing AISUKF framework are experimented and evaluated one at a time to determine the suitable model to enhance the framework. The experimental outcome and interpretations from the results are discussed in Section IV.

## IV. RESULTS AND DISCUSSION

### A. Data and Experimental Setup

The proposed method has been experimented on both synthetic images and real SAR images. Sentinel-1 C-band SAR images acquired between February 2020 and June 2020 [16] over Bay of Naples, Italy (see Fig. 3 SAR Image 1), and over regions of Al Foah, United Arab Emirates (see Fig. 3 SAR Image 2), are taken as real SAR images.

The synthetic images shown in Fig. 1, indicated as Original, are initially downsampled to size  $(128 \times 128)$  and degraded with speckle (Rayleigh distribution [17]) and translational motion to mimic the captured real SAR images. These are then reconstructed to its original resolution of size  $(256 \times 256)$  in order to evaluate the proposed work with reference to the ground truth. The number of multiple LR images used for synthetic image SR is 16, whereas, for real SAR image SR, we have used 12 LR images. The following full-reference assessment metrics, namely, peak-signal to noise ratio (PSNR), structural similarity index metric (SSIM), feature similarity index metric (FSIM), and edge preservation factor (EPF) metrics [9], are used to evaluate our proposed technique with other existing techniques of Yang *et al.* [2] [SR using sparse representation (ScSR)],

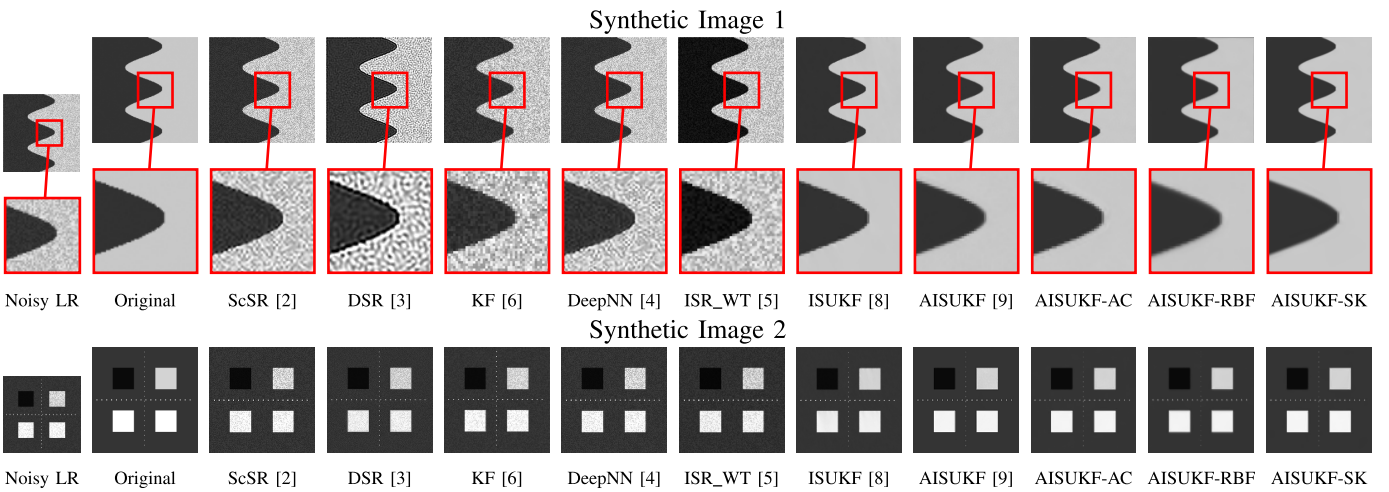


Fig. 1. SR result of various techniques on noisy synthetic images with noise variance of 0.01.

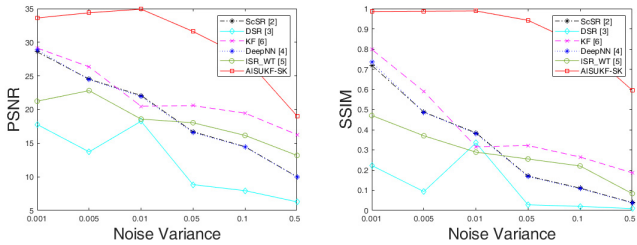


Fig. 2. Plots show (left) PSNR and (right) SSIM as functions of noise variance.

TABLE I  
PERFORMANCE EVALUATION OF SR ON SYNTHETIC IMAGE 1

	PSNR	SSIM	FSIM	EPF
Yang et al. [2]	22.1	0.3847	0.8842	0.4539
Dong et al. [3]	18.3	0.3349	0.8900	0.4809
Wei et al. [6]	20.5	0.2013	0.3531	0.3002
Wang et al. [4]	21.9	0.3810	0.8842	0.3972
Shkvarko et al. [5]	18.6	0.2858	0.8389	0.3894
Kanakaraj et al. [8]	31.6	0.9797	0.9932	0.7455
Kanakaraj et al. [9]	32.7	0.9841	0.9943	0.7931
AISUKEF - AC kernel	33.8	0.9843	<b>0.9946</b>	0.7616
AISUKEF - RBF kernel	27.8	0.9650	0.9896	0.7962
AISUKEF - Steering kernel	<b>34.9</b>	<b>0.9888</b>	0.9903	<b>0.8647</b>

Dong *et al.* [3] [combined deblurring and SR (DSR)], Wei *et al.* [6] (KF), Wang *et al.* [4] (DeepNN), Shkvarko *et al.* [5] (ISR\_WT), Kanakaraj *et al.* [8] (ISUKEF), and Kanakaraj *et al.* [9] (AISUKEF) who perform SR. In real SAR images, the resolution of the image is directly upsampled by a factor of 2 without the degradation step, as in practical applications. We have used two no-reference assessment metrics: the equivalent number of looks (ENLs) [9] to evaluate the level of denoising and the Distortion Identification-based Image Verity and INtegrity Evaluation (DIIVINE) index [18] to evaluate the preservation of the structural details in the super-resolved output image.

### B. Analysis

Tables I and II present the quality assessment metric values of SR on the synthetic images shown in Fig. 1. In comparison with other proposed kernel methods, the quantitative results of using the AISUKEF with SK (AISUKEF-SK) gives better denoising values compared with the AC kernel and RBF

TABLE II  
PERFORMANCE EVALUATION OF SR ON SYNTHETIC IMAGE 2

	PSNR	SSIM	FSIM	EPF
Yang et al. [2]	22.8	0.5628	0.5105	0.1515
Dong et al. [3]	25.1	0.1953	0.5499	<b>0.6455</b>
Wei et al. [6]	23.9	0.1645	0.6537	0.1586
Wang et al. [4]	23.1	0.5624	0.8793	0.2234
Shkvarko et al. [5]	23.1	0.1427	0.6078	0.1130
Kanakaraj et al. [8]	27.9	0.9455	0.9609	0.5034
Kanakaraj et al. [9]	28.5	0.9554	0.9955	0.5124
AISUKEF - AC kernel	28.6	<b>0.9579</b>	0.9962	0.5387
AISUKEF - RBF kernel	26.5	0.9343	0.9936	0.4011
AISUKEF - Steering kernel	<b>28.8</b>	0.9562	<b>0.9967</b>	0.5162

kernel. An increase of 1.1 dB in the PSNR value of the AISUKEF-SK regression has been observed. In addition, the EPF value of 0.8647 demonstrates better edge preservation. Visual examination of the SR result of AISUKEF-SK (zoomed) on Synthetic image 1 shows better preservation of edges and is free of artifacts. SR result of AISUKEF-SK technique on synthetic image 2 in Fig. 1 shows smoother homogeneous regions compared with the existing AISUKEF technique result. We have also tested the SR performance with different levels of noise, and the resulting values for PSNR and SSIM metrics, as plotted in Fig. 2, indicate the remarkable performance for our proposed method compared with other works from the literature.

The ENL values in Table III are computed from the region R1 and R2 of SAR image 1 and SAR image 2, respectively. These regions are marked and enlarged in the SR outputs in Fig. 3. The ENL values of input SAR images are 2.138 for R1 (SAR image 1) and 4.6774 for R2 (SAR image 2). The SR technique by Dong *et al.* [3] shows the highest value for the DIIVINE index in Table III. The high noise content may be observed from the zoomed-in portion of the images, indicating low ENL values for the same. The noise in this image is considered as a textured pattern, thereby resulting in a high DIIVINE index. The ENL value for our proposed method is 74.5 for SAR image 1 and 2112.5 for SAR image 2, indicating high noise suppression. Also, the high DIIVINE index shows structural detail preservation. A higher value for the combination of ENL and DIIVINE

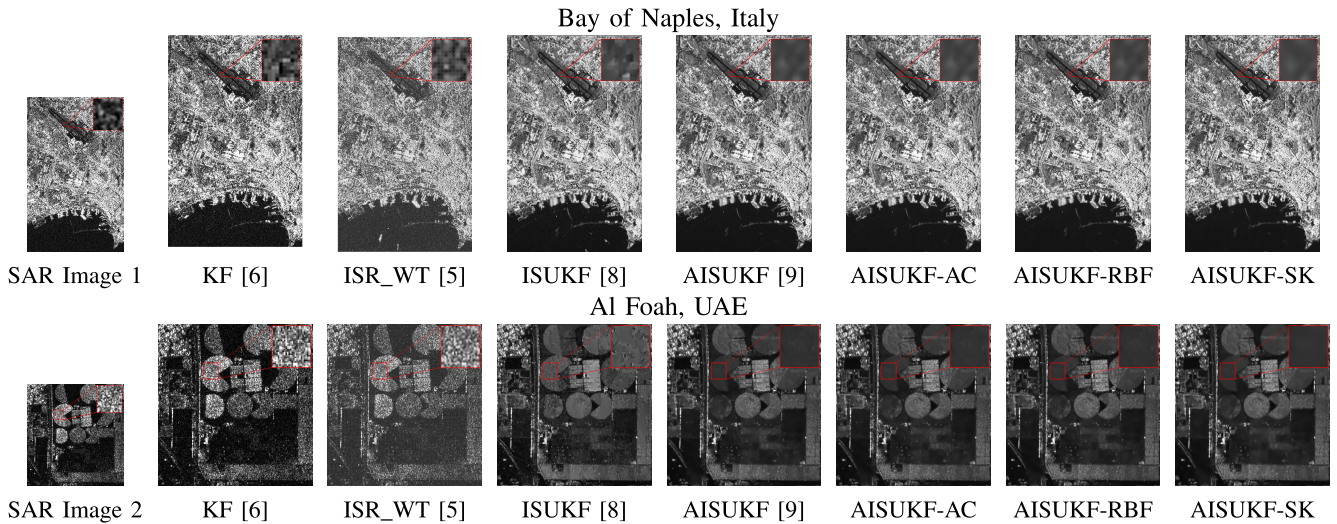


Fig. 3. SR results on SAR Image 1 and SAR Image 2 using various techniques.

TABLE III  
PERFORMANCE EVALUATION ON REAL SAR IMAGES

	SAR Image 1	SAR Image 2		
	ENL(R1)	DIIVINE	ENL(R2)	DIIVINE
Yang et al. [2]	2.1	64.2	3.6	17.8
Dong et al. [3]	0.8	71.0	1.3	70.9
Wei et al. [6]	2.9	33.5	4.7	17.8
Wang et al. [4]	3.9	46.5	4.3	13.6
Shkvarko et al. [5]	7.4	43.5	8.2	5.2
Kanakaraj et al. [8]	8.0	29.1	44.8	23.1
Kanakaraj et al. [9]	56.8	25.1	483.7	20.4
AISUKF - AC kernel	59.2	25.2	492.7	20.6
AISUKF - RBF kernel	56.3	25.3	516.0	20.4
<b>AISUKF - Steering kernel</b>	<b>74.5</b>	<b>26.6</b>	<b>2112.5</b>	<b>23.1</b>

index shows the superiority of the proposed AISUKF-SK model. A visual examination of the images in Figs. 1 and 3 along with the values in Tables I–III reveals noise reduction and more structural preservation after the reconstruction using our proposed framework.

## V. CONCLUSION

This letter proposes a novel method to improve the existing AISUKF for SAR image SR. The procedure can simultaneously denoise and super-resolve SAR images that are inherently affected by speckle. Adding a compensation value, derived through kernel regression, to the final estimate from the AISUKF framework has proved to be beneficial. We have compared three different nonlinear kernel regression models and concluded that the SK regression model is the most suitable nonlinear kernel for the regression technique incorporated into the AISUKF for SAR image SR. The SK regression-based SR output reveals more noise reduction and also better preservation of edges and other fine details in the image.

## REFERENCES

- X. Zhang, K. Cao, and L. Jiao, “A contourlet-based interpolation restoration method for super-resolution of SAR image,” in *Proc. 2nd Asian-Pacific Conf. Synth. Aperture Radar*, Oct. 2009, pp. 1068–1071.
- J. Yang, J. Wright, T. S. Huang, and Y. Ma, “Image super-resolution via sparse representation,” *IEEE Trans. Image Process.*, vol. 19, no. 11, pp. 2861–2873, Nov. 2010.
- W. Dong, L. Zhang, G. Shi, and X. Wu, “Image deblurring and super-resolution by adaptive sparse domain selection and adaptive regularization,” *IEEE Trans. Image Process.*, vol. 20, no. 7, pp. 1838–1857, Jul. 2011.
- Z. Wang, D. Liu, J. Yang, W. Han, and T. Huang, “Deep networks for image super-resolution with sparse prior,” in *Proc. IEEE Int. Conf. Comput. Vis. (ICCV)*, Dec. 2015, pp. 370–378.
- Y. V. Shkvarko, J. I. Yanez, J. A. Amao, and G. D. M. del Campo, “Radar/SAR image resolution enhancement via unifying descriptive experiment design regularization and wavelet-domain processing,” *IEEE Geosci. Remote Sens. Lett.*, vol. 13, no. 2, pp. 152–156, Feb. 2016.
- Z. Wei, F. Tao, and W. Jun, “Kalman filter-based method for image superresolution using a sequence of low-resolution images,” *J. Electron. Imag.*, vol. 23, no. 1, pp. 013008(1)–013008(12), 2014.
- F. Dellaert, S. Thrun, and C. Thorpe, “Jacobian images of super-resolved texture maps for model-based motion estimation and tracking,” in *Proc. 4th IEEE Workshop Appl. Comput. Vis.*, Oct. 1998, pp. 2–7.
- S. Kanakaraj, M. S. Nair, and S. Kalady, “SAR image super resolution using importance sampling unscented Kalman filter,” *IEEE J. Sel. Topics Appl. Earth Observ. Remote Sens.*, vol. 11, no. 2, pp. 562–571, Feb. 2018.
- S. Kanakaraj, M. S. Nair, and S. Kalady, “Adaptive importance sampling unscented Kalman filter based SAR image super resolution,” *Comput. Geosci.*, vol. 133, Dec. 2019, Art. no. 104310.
- G. R. K. S. Subrahmanyam, A. N. Rajagopalan, and R. Aravind, “A recursive filter for despeckling SAR images,” *IEEE Trans. Image Process.*, vol. 17, no. 10, pp. 1969–1974, Oct. 2008.
- H. Takeda, S. Farsiu, and P. Milanfar, “Kernel regression for image processing and reconstruction,” *IEEE Trans. Image Process.*, vol. 16, no. 2, pp. 349–366, Feb. 2007.
- M. Guizar-Sicairos, S. T. Thurman, and J. R. Fienup, “Efficient subpixel image registration algorithms,” *Opt. Lett.*, vol. 33, no. 2, pp. 156–158, 2008.
- X. Liu, M. Tanaka, and M. Okutomi, “Single-image noise level estimation for blind denoising,” *IEEE Trans. Image Process.*, vol. 22, no. 12, pp. 5226–5237, Dec. 2013.
- C. Jojj, M. S. Nair, G. R. K. S. Subrahmanyam, and R. Riji, “Discontinuity adaptive non-local means with importance sampling unscented Kalman filter for de-speckling SAR images,” *IEEE J. Sel. Topics Appl. Earth Observ. Remote Sens.*, vol. 6, no. 4, pp. 1964–1970, Aug. 2013.
- Y. Cho and L. K. Saul, “Kernel methods for deep learning,” in *Proc. Adv. Neural Inf. Process. Syst.*, 2009, pp. 342–350.
- European Space Agency. *Sentinel Online: Data Products*. Accessed: Jun. 13, 2020. [Online]. Available: <https://sentinel.esa.int/web/sentinel/missions/sentinel-1/data-products/>
- E. E. Kuruoglu and J. Zerubia, “Modeling SAR images with a generalization of the Rayleigh distribution,” *IEEE Trans. Image Process.*, vol. 13, no. 4, pp. 527–533, Apr. 2004.
- A. K. Moorthy and A. C. Bovik, “Blind image quality assessment: From natural scene statistics to perceptual quality,” *IEEE Trans. Image Process.*, vol. 20, no. 12, pp. 3350–3364, Dec. 2011.